Driven Random Dynamic Reservoir with Homeostatic Variance Control

1 Model Description

1.1 Dynamics

$$x_i^{t+1} = \tanh\left(g_i^t I_i^{t+1}\right) \tag{1}$$

$$I_i^{t+1} = \sum_{j=1}^{N_{\text{net}}} W_{ij} x_j^t + W_i^E E_i^{t+1} \tag{2}$$

$$g_i^{t+1} = g_i^t + \mu_g \left[\sigma_{\text{target}}^2 - \left(x_i^t - \langle x_i \rangle\right)^2\right] \tag{3}$$

1.2 Parameters / Settings

W_{ij} is a sparse random matrix with connection probability cf_{net}. Nonzero entries were drawn from a Gaussian distribution $\mathcal{N}(\mu = 0, \sigma = \sigma_{\text{conn}}/\sqrt{N_{\text{net}}\text{cf}_{\text{net}}})$. Diagonal entries were always set to zero.

E_i^t are random vectors of size N_{net} with independent entries drawn from a Gaussian distribution $\mathcal{N}(\mu = 0, \sigma = \sigma_{\text{ext}})$. Similarly, W_i^E is a random vector of size N_{net}, drawn from $\mathcal{N}(\mu = 0, \sigma = \sigma_{\text{W}^{\text{E}}})$. External input is turned off after $t_{\text{ext.off}}$.

By changing individual gain values g_i, the homeostatic control tries to drive the activity standard deviation of every cell to the value given by σ_{target}. However, this mechanism is also switched off after $t_{\text{ext.off}}$. This is done because we can assume that homeostatic processes would biologically act on much slower timescales than changes in input. Before $t_{\text{ext.off}}$, we can set μ_g to relatively high values to let homeostasis converge under external drive.

See all parameters in Table 1.

Table 1: Model Parameters

Parameter	N_{net}	cf_{net}	σ_{conn}	σ_{ext}	$\sigma_{\text{W}^{\text{E}}}$	μ_g	σ_{target}	n_t (Sim. Steps)	$t_{\text{ext.off}}$
Value	500	0.1	1.0	1.0	1.0	$5 \cdot 10^{-4}$	0.33	$2 \cdot 10^5$	10^5

2 Derivation of Gain Dynamics from Objective Function

We would like to justify our choice of (3) by deriving an update rule from a suitable objective function F_σ:

$$F_\sigma = \left[\left\langle \left(x - \langle x \rangle_T\right)^2 \right\rangle_T - \sigma_{\text{target}}^2\right]^2 \tag{4}$$

Using $\Delta g \propto -\frac{\partial F_\sigma}{\partial g}$:

$$\Delta g \propto g^{-1} \left[\sigma_{\text{target}}^2 - \left\langle \left(x - \langle x \rangle_T\right)^2 \right\rangle_T\right] \left\langle \left(x - \langle x \rangle_T\right) \operatorname{arctanh}(x) \left(1 - x^2\right) \right\rangle_T \tag{5}$$

$$= g^{-1} \left[\sigma_{\text{target}}^2 - \left\langle \left(x - \langle x \rangle_T\right)^2 \right\rangle_T\right] \text{Cov}\left[x, \operatorname{arctanh}(x) \left(1 - x^2\right)\right]_T \tag{6}$$

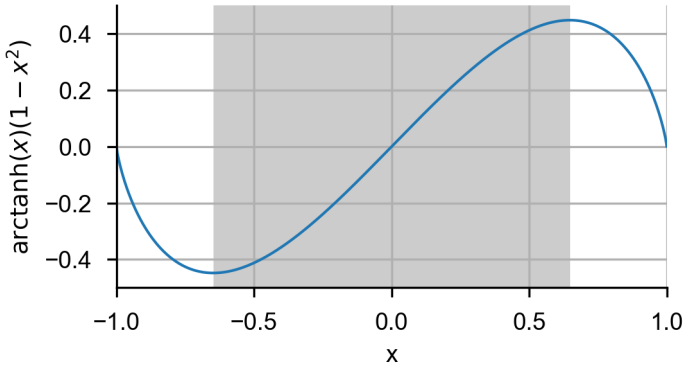

Figure 1: Covariance term of (6). If x is bound within the gray area, positive cov. is ensured.

The sign in the covariance term in (6) determines whether the dynamics given in (3) are recovered, or if the gain adaptation is reversed. Intuitively, it indicates if increasing g broadens or narrows the output distribution. Fig. 1 illustrates that a positive covariance is always ensured if the activity remains within the region highlighted in gray, which is approximately given by $(-0.648, 0.648)$. For symmetry reasons, $\mathrm{Cov}\left[x, \mathrm{arctanh}(x)\left(1-x^2\right)\right]_T \geq 0$ also holds for distributions exceeding this bound if they are symmetric around $x = 0$. In our numerical simulations, this symmetry condition was fulfilled due to the Gaussian distribution of the neural input, which was centered around zero. This allowed us to reduce dynamics to the essential term $\left[\sigma^2_{\text{target}} - \left\langle (x - \langle x \rangle_T)^2 \right\rangle_T\right]$.

3 Results

Exemplary results are shown in Fig. 2.

4 Mean Field Approximation

We would like to find an approximate relation between the gain resulting from homeostasis and the input and target variance. In the following, we shall denote by $\langle \cdot \rangle_T$ an average over time and by $\langle \cdot \rangle_P$ over the population. If we linearize the neural activation function and take an average over time, we get

$$\langle x_i^2 \rangle_T = g_i^2 \left\langle \left(\sum_{j=1}^{N_{\text{net}}} W_{ij} x_j + E_i \right)^2 \right\rangle_T \tag{7}$$

$$= g_i^2 \left\langle \left(\sum_{j=1}^{N_{\text{net}}} W_{ij} x_j \right)^2 \right\rangle_T + g_i^2 E_i^2 \tag{8}$$

$$= g_i^2 \sum_{j,k=1}^{N_{\text{net}}} W_{ij} W_{ik} \langle x_j x_k \rangle_T + g_i^2 E_i^2 \ . \tag{9}$$

If we assume that the system is in a chaotic state we can set $\langle x_j x_k \rangle_T = 0$ for $j \neq k$. This leads to

$$\langle x_i^2 \rangle_T = g_i^2 \left(\sum_{j=1}^{N_{\text{net}}} W_{ij}^2 \langle x_j^2 \rangle_T + \sigma^2_{\text{ext}} \right) \tag{10}$$

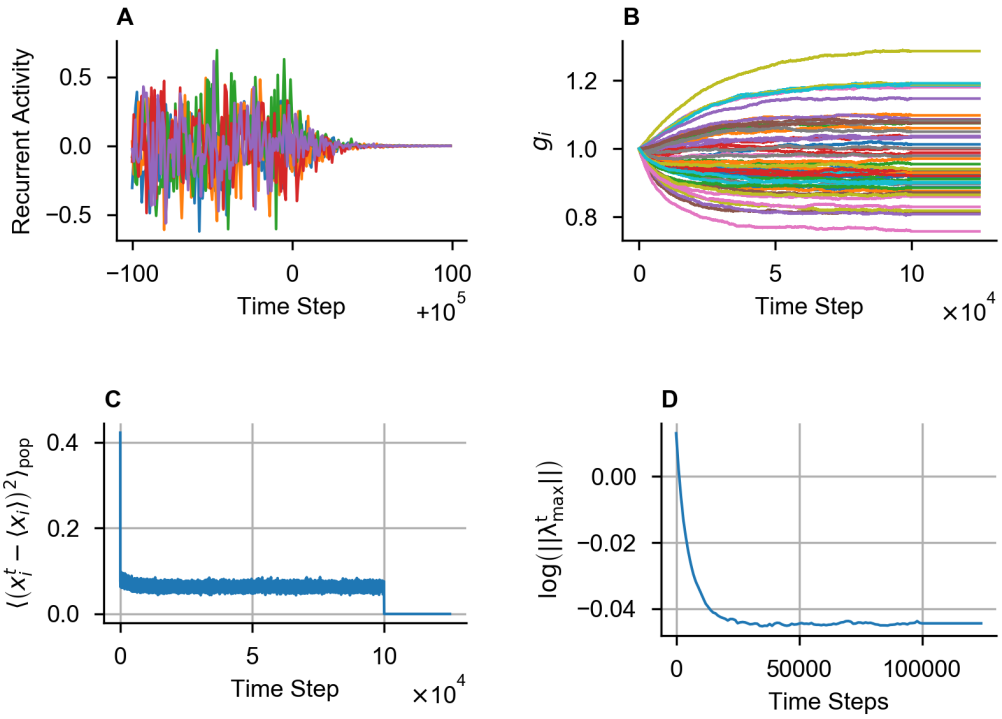

Figure 2: **A**: Sample of activity within $[t_{\text{ext.off}} - 100, t_{\text{ext.off}} + 100]$. **B**: Gain dynamics of $N_{\text{net}}/10$ exemplary neurons. **C**: Population mean of squared activity. **D**: Log. of largest absolute value of eigenvalues of $g_i^t W_{ij}$.

where we have assumed $\langle E_i \rangle_T = 0$ for all i.

By design, our homeostatic mechanism fixes all $\langle x_i^2 \rangle_T$ to σ^2_{target}. Thus,

$$\sigma^2_{\text{target}} = g_i^2 \left(\sigma^2_{\text{target}} \sum_{j=1}^{N_{\text{net}}} W_{ij}^2 + \sigma^2_{\text{ext}} \right) \tag{11}$$

$$g_i = \left(\sum_{j=1}^{N_{\text{net}}} W_{ij}^2 + \sigma^2_{\text{ext}} / \sigma^2_{\text{target}} \right)^{-1/2} . \tag{12}$$

Since W_{ij} is a random Gaussian matrix with variance $\sigma^2_{\text{conn}} / (N_{\text{net}} c f_{\text{net}})$, $\sum_{j=1}^{N_{\text{net}}} W_{ij}^2$ follows a χ^2 - distribution with variance $\frac{2 N_{\text{net}} c f_{\text{net}} \sigma^2_{\text{conn}}}{N^2_{\text{net}} c^2 f^2_{\text{net}}} = \frac{2\sigma^2_{\text{conn}}}{N_{\text{net}} c f_{\text{net}}}$. For $N_{\text{net}} \to \infty$, its variance vanishes and consequently, all g_i converge to the same value, namely

$$g = \left(\sigma^2_{\text{conn}} + \sigma^2_{\text{ext}} / \sigma^2_{\text{target}} \right)^{-1/2} . \tag{13}$$

This equation predicts that g should not change if the ratio between target and input variance remains constant. We ran a parameter sweep over σ_{ext} and σ_{target} with a network of $N_{\text{net}} = 1000$ neurons and looked at the resulting distribution of gains and the maximal Lyapunov exponent. Importantly, this approximation suggests that the network should tune into a subcritical configuration for any non-vanishing external input. Even though this is not strictly verified in the numerical simulation, see Fig. 3A, it holds for the majority of $\sigma_{\text{ext}}/\sigma_{\text{target}}$ combinations.

4.1 Self-Consistency Equation with Full Activation Function

If we do not restrict ourself to a linearized version of the activation function, (7) becomes

$$\left\langle x_i^2 \right\rangle_T = \left\langle \tanh\left(g_i \left(\sum_{j=1}^{N_{\text{net}}} W_{ij} x_j + E_i \right) \right)^2 \right\rangle_T . \tag{14}$$

Again, assuming that $\langle x_j x_k \rangle_T = 0$ for $j \neq k$ and $N_{\text{net}} \to \infty$, the sum of weight and inputs follows a Gaussian distribution $\mathcal{N}\left(\mu = 0, \sigma = \sqrt{\sigma_{\text{conn}}^2 \sigma_{\text{target}}^2 + \sigma_{\text{ext}}^2}\right)$. Replacing the time average with an integral over the distribution of the input, we arrive at the full self-consistency equation

$$\sigma_{\text{target}}^2 = \int_{-\infty}^{\infty} \tanh^2(gx)\, \mathcal{N}\left(x, \mu = 0, \sigma = \sqrt{\sigma_{\text{conn}}^2 \sigma_{\text{target}}^2 + \sigma_{\text{ext}}^2}\right) \mathrm{d}x \tag{15}$$

As a second order approximation with respect to tanh, we can use $\tanh^2(x) \approx x^2 - \frac{2}{3}x^4$ in the integral, which gives

$$\begin{aligned}
\sigma_{\text{target}}^2 &\approx \frac{1}{g\sqrt{2\pi}\sigma_{\text{total}}} \int_{-\infty}^{\infty} \left(x^2 - \frac{2}{3}x^4 \right) \exp\left(\frac{-x^2}{2g^2\sigma_{\text{total}}^2} \right) \mathrm{d}x && (16)\\
&= g^2\sigma_{\text{total}}^2 - 2g^4\sigma_{\text{total}}^4 && (17)\\
&= g^2\left(\sigma_{\text{conn}}^2\sigma_{\text{target}}^2 + \sigma_{\text{ext}}^2\right) - 2g^4\left(\sigma_{\text{conn}}^2\sigma_{\text{target}}^2 + \sigma_{\text{ext}}^2\right) && (18)
\end{aligned}$$

where we have defined $\sigma_{\text{total}} = \sqrt{\sigma_{\text{conn}}^2 \sigma_{\text{target}}^2 + \sigma_{\text{ext}}^2}$ for convenience. Note that neglecting the second term on the right hand side of (18) reduces the equation to (13). Since this first order approximation does not explain the $g = 1$ transition traced in Fig. 3B as a dashed blue line, we were particularly interested in the solution of (18) for $g = 1$. Moreover, we set $\sigma_{\text{conn}} = 1$ as in the simulations. We therefore had to solve

$$\sigma_{\text{target}}^4 + \sigma_{\text{ext}}^4 + 2\sigma_{\text{target}}^2\sigma_{\text{ext}}^2 - \frac{\sigma_{\text{ext}}^2}{2} = 0 . \tag{19}$$

This equation can be rearranged to

$$\left[\left(\sigma_{\text{ext}} - \frac{1}{\sqrt{8}} \right)^2 + \sigma_{\text{target}}^2 - \frac{1}{8} \right] \left[\left(\sigma_{\text{ext}} + \frac{1}{\sqrt{8}} \right)^2 + \sigma_{\text{target}}^2 - \frac{1}{8} \right] = 0 . \tag{20}$$

From this form we can see that the solution set consists of two circles with radius $1/\sqrt{8}$ in the σ_{target}, σ_{ext} space, centered around $\sigma_{\text{target}} = 0$, $\sigma_{\text{ext}} = \pm 1/\sqrt{8}$. Fig. 4 shows a comparison between this approximation and the simulation.

5 Behavior for Input with Correlations Across Time/Population

Test with e.g. Ornstein-Uhlenbeck Process and/or dominant princ. comp. in input space

6 Related Literature

The effect of homoestatic mechanisms onto echo state network performance has been investigated in several works. A common approach derives dynamic adaptation rules from

the minimization of a functional (usually KL-divergence) of an empirical estimate of each neuron's output distribution and a target PDF [Triesch (2007); Schrauwen et al. (2008); Boedecker et al. (2009)].

To be extended

References

Boedecker, J., Obst, O., Mayer, N. M., and Asada, M. (2009). Initialization and self-organized optimization of recurrent neural network connectivity. *HFSP Journal*, 3(5):340–349.

Schrauwen, B., Wardermann, M., Verstraeten, D., Steil, J. J., and Stroobandt, D. (2008). Improving reservoirs using intrinsic plasticity. *Neurocomputing*, 71(7-9):1159–1171.

Triesch, J. (2007). Synergies Between Intrinsic and Synaptic Plasticity Mechanisms. *Neural Computation*, 19(4):885–909. PMID: 17348766.

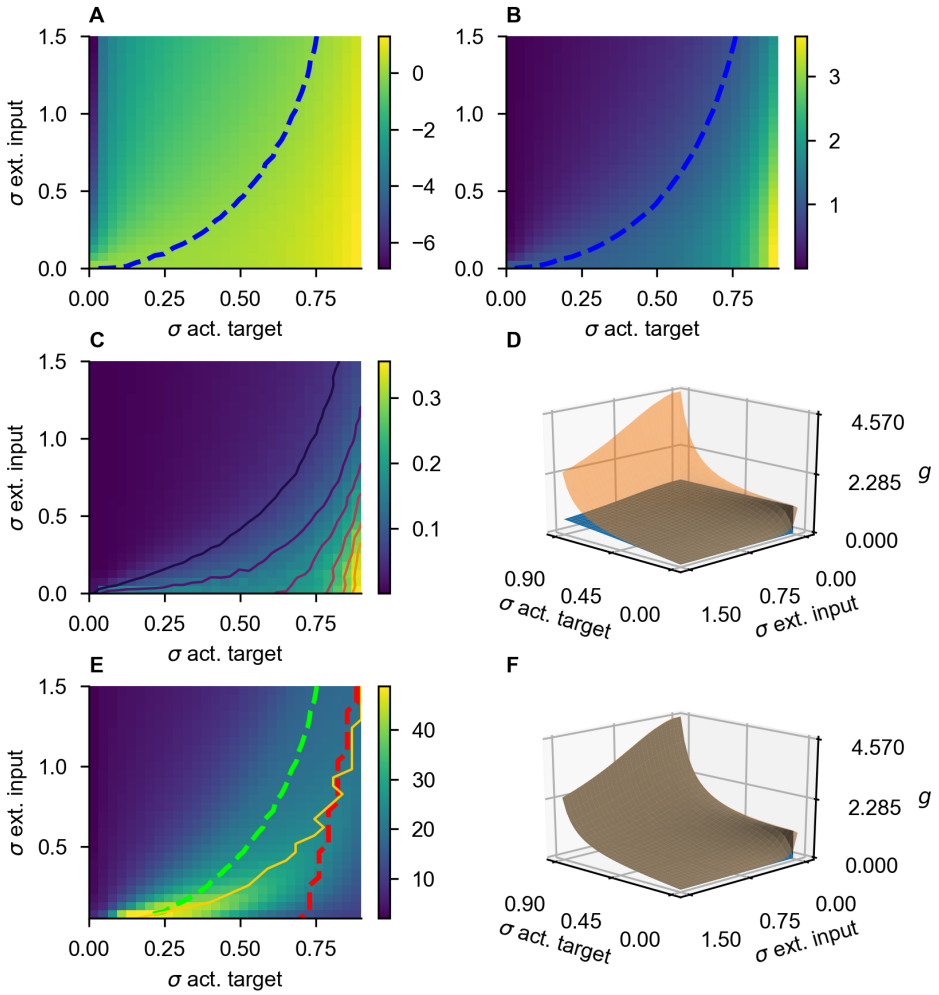

Figure 3: Parameter sweep, run on a network with $N_{\text{net}} = 1000$. **A**: Log of largest absolute value of eigenvalues of $g_i W_{ij}$. Blue dashed line marks the zero transition. **B** : $\langle g_i \rangle_P$. Blue dashed line marks the $\langle g_i \rangle_P = 1$ transition. **C**: $\left\langle (g_i - \langle g_i \rangle_P)^2 \right\rangle_P$. **D**: Prediction of (13) (blue) and numerical result (orange) of $\langle g_i \rangle_P$. **E**: Memory Capacity (color coded), transition $\langle g_i \rangle_P = 1$ (green line), maximal memory capacity for a given standard deviation of external drive (orange). Red line marks the loss of the echo state property (!!!!Might be wrong!!!!). **F**: $\langle g_i \rangle_P$ from the simulation matches the numerically determined solution of (15).

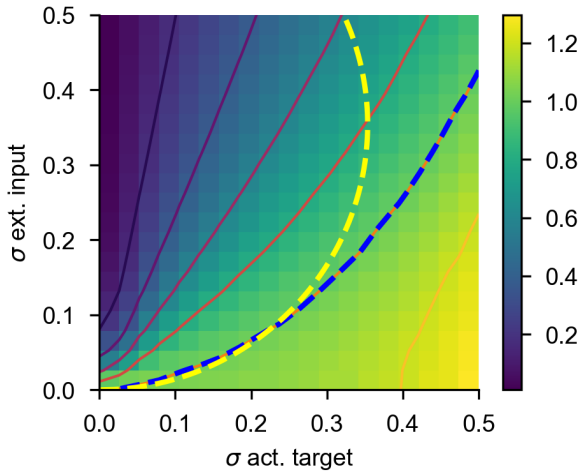

Figure 4: Comparison of the $\langle g_i \rangle_P = 1$ transition (blue) shown in Fig. 3B and the second order approximate solution (yellow) given by (20).